Cutting nanodisks in graphene down to 20 nm in diameter

Makoto Sakurai*[1], Ayako Omura Okano[2], Takuya Iwasaki[1] and Christian Joachim[3,1]

[1]Research Center for Materials Nanoarchitectonics (WPI-MANA), National Institute for Materials Science (NIMS), 1-1 Namiki, Tsukuba, Ibaraki 305-0044, Japan

[2]Tsukuba University, Tsukuba, Ibaraki 305-8577, Japan

[3]Centre d'Elaboration de Matériaux et d'Études Structurales (CEMES), Centre National de la Recherche Scientifique (CNRS), 29 Rue J. Marvig, BP 4347, 31055 Toulouse Cedex, France

Received xxxxxx
Accepted for publication xxxxxx
Published xxxxxx

Abstract

A direct focused He^+ beam direct machining is presented to fabricate solid-state nano-disk at the surface of a graphene multilayer micro-flake deposited on an Au/Ti/sapphire surface. At irradiation doses larger than 5.0×10^{17} ions/cm^2 and with a beam size well below 1 nm, graphene disks down to 20 nm in diameter have been machined with for nano-disk down to 50 nm in diameter, a central hole for preparing the positioning of a rotation axle. The local heat generated by this irradiation is inducing a partial graphene amorphization and deformation, leading to a complete graphene nano-disk vaporization at doses larger than 5×10^{18} ions/cm^2. A dry transfer printing technique followed by a graphene surface cleaning was used to transfer the nano-disks from its initial surface to a fresh and clean surface. Tapping mode atomic force micrograph has been recorded to follow the vaporization as a function of the He^+ dose to confirm the graphene solid-state nano-disk fabrication limit to about 20 nm with this process.

Keywords: Focused He ion beam, scanning helium microscope, Tapping mode AFM, heat generation, solid-state nanodisks, graphene

Color printing only online

1. Introduction

Solid state nano-gears and nano-disks are of fundamental interest for the construction of nanoscale mechanical machinery immune to radiations [1], to mechanically interface a single molecule logic gate for mechanical data inputs [2] and to transfer rotational motion to a single molecule-gears train [3,4] or a single molecule-motor [5,6]. A central hole is also required to mount each of them on a robust nanoscale rotation axle. For those mechanical interfaces, nanoscale teeth around the nano-disk edge of the gear are not required. The native molecular scale corrugation at the nano-disk edge will normally be enough for the transmission of a rotation between the solid-state nano-disk and a single molecule machinery as recently simulated using molecular dynamics [7]. This is important to consider since nanofabrication of teeth with a width below 5 nm are very difficult to achieve [8,9]. At the same time, the nano-disk thickness must be at the atomic scale to be compatible with the nanometer van der Waals thickness of for example a molecule-gear. This is calling for their fabrication using two-dimensional (2D) nanomaterials like graphene. Recently, we have shown how a graphene solid state nano-gear and also a nano-disk can be machined down to

 © xxxx IOP Publishing Ltd

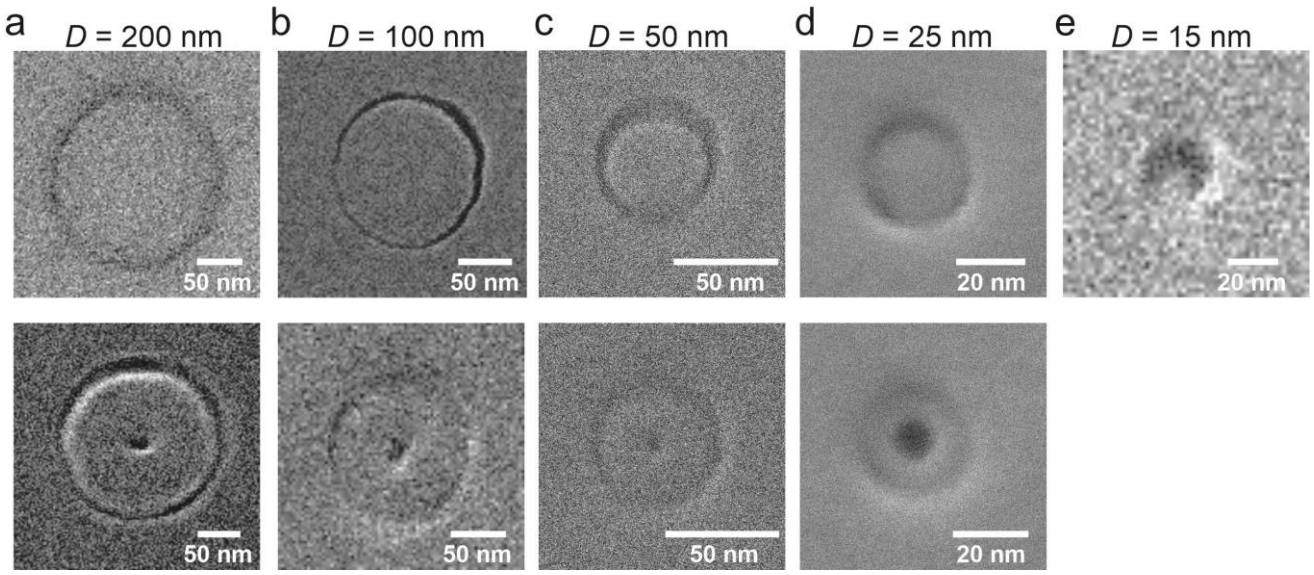

Figure 1. A series of nano-disks with their central hole going from 200 nm to almost 15 nm in diameter using HIM imaging at low dose. Notice that the central hole for 25 nm was machined by only leaving the He^+ at a fix position in the centre of the graphene nano-disk to demonstrate the difference between this strategy and the line-by-line strategy used for 200 nm, 100 nm and 50 nm for the other presented nano-disks in the second raw.

30 nm in diameter using the extremely well focused ions beam of an He^+ microscope (HIM) [10]. Standard Ga^+ focused ion beams (FIB) [11] and e-beam with resist [8] or HIM nano-lithography also with resist [12] are unable to reach such nano-disk diameter nor to fabricate atomic scale in thickness solid state nano-disks.

In this paper, we report the complete fabrication process of graphene nano-disks for nano-mechanics pushing the He^+ cutting technique to its limits on graphene. After the description of our He^+ machining on graphene in section 2.1, an in-air transfer protocol is presented in section 2.2 to bring a single machined graphene flake with its nano-disks on a fresh Au/Ti/sapphire wafer surface. Then, a careful cleaning protocol of the surface of the transferred graphene flake was developed to be able to atomic force microscopy (AFM) image the nano-disks. These AFM images are presented in section 2.3 to be compared with their low dose HIM counterparts recorded before this transfer. This second characterization is demonstrating the exothermicity of our He^+ machining process. Since the graphene lattice is He^+ bombarded at high doses for the cutting, this machining is locally generating heat [9,10] like with the standard Ga^+ FIB or in any macroscopic machining process. The structural change in the graphene in the nano-disk by the heat is discussed in section 3 according to the known macroscopic carbon materials thermodynamic triple point. In the section 4 conclusion, we comment on the optimum He^+ dose to be used for nano-disk surface machining as a function of the targeted graphene nano-disk diameter and on a possible choice of another 2D lamellar nanomaterial.

2. Results

2.1. The HIM graphene nano-cutting process

Atomically flat c(0001) sapphire 5 mm × 10 mm in lateral dimension wafers (Shinkosha Co., Kanagawa, Japan) were

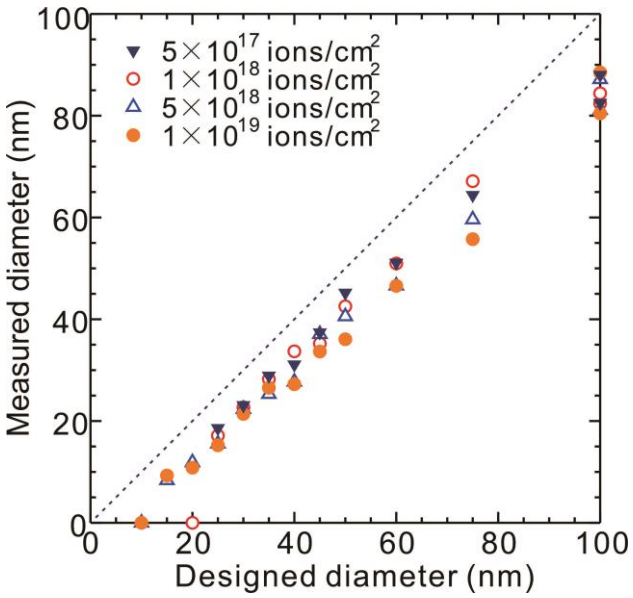

Figure 2. The variation of the HIM image measured graphene nano-disk diameters as a function of the programmed He^+ irradiation circle diameter *D* for 4 different He^+ doses ranging from 5.0 $\times 10^{17}$ to 1.0 $\times 10^{19}$ ions/cm^2. The width of the cut i.e., the number of lateral 0.35 nm in diameter pixels was 1 nm for all the dose and nano-disk diameter. For very low diameter typically below 50 nm, a decrease of the number of pixels was programmed to reduce the dose. The effect of this reduction is exemplified in figure 3.

used as a support for the graphene He^+ nano-cutting process. With an average 20 µm lateral size and a 100 nm thickness, graphene flakes were scotch-tap exfoliated from a HOPG graphite surface onto this Au(20 nm)/Ti(5 nm)/sapphire surface. The 20 nm thick Au layer was necessary to evacuate charges and to avoid the sapphire surface deformation during the nano-disk sculpturing [13]. The 100 nm graphene thickness was selected on purpose to avoid a complete vaporization of nano-disks below 50 nm in diameter and to limit the lateral deformation of the graphene surface under the He^+ cutting stress (See figure 9). As presented in section 2.3 using AFM imaging, the depth of the cutting is self-limited to a maximum of 80 nm (see also section 3 for discussion). After the cutting and the fabrication of a central hole, the He^+ machined graphene flake was in-air transfer on a fresh new Au(20 nm)/Ti(5 nm)/sapphire surface as described in section 2.2. For the section 2.3 TEM electron diffraction experiments, a CVD bilayer graphene transferred on a Si_3N_4 TEM grid was used for an independent He^+ nano-cutting process**.**

Our Orion Plus helium ion microscope (HIM) (Zeiss, Peabody, USA) is operating at an acceleration voltage of 30 keV to irradiate focussed He^+ beams at the surface of the sapphire wafer. The Orion chamber pressure during the machining was 1.02×10^{-6} Torr. HIM images were recorded with doses between 4 and 8×10^{15} ions/cm^2, about two orders of magnitude below the He^+ irradiation machining threshold on the graphene surface. The spatial lateral extension of our He^+ beam is 0.35 nm in diameter [10]. On the graphene flake surface, the He^+ beam cutting trajectory was controlled by the Orion patterning software allowing a minimum 1 nm pixel spacing for irradiation in each direction on the surface. For the cutting, the electronically generated circle mask is composed of a series of He^+ beam scan lines perpendicular to the target circle, each line being separated 1 nm one after the other. The number N of pixels per line was changed according to the relation $N = 0.08\ D$ with D the targeted circle diameter. This relation was determined after different tests where for example

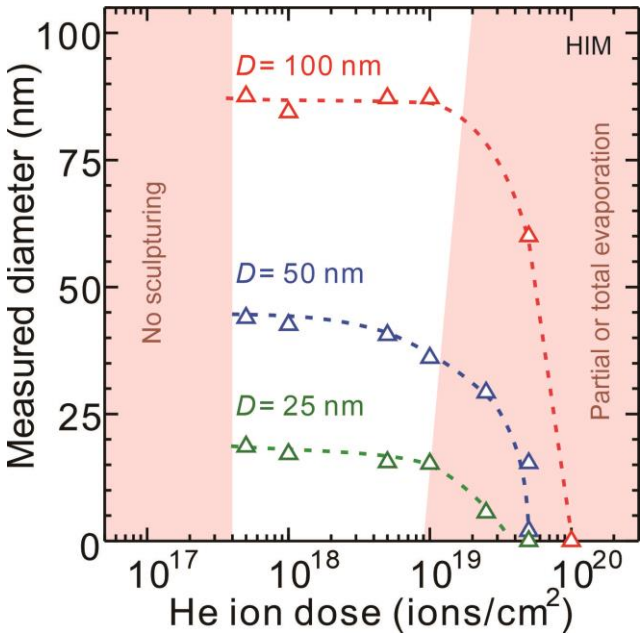

Figure 3. The variation of the HIM image measured graphene nano-disk diameters as a function of the dose for three characteristics diameters D: 100 nm, 50 nm, and 25 nm. Graphene nano disk vaporize for doses larger than 3.0×10^{19} ions/cm^2.To preserve the nano-disk by minimizing the linewidth of the cut at low diameters, there is no cut below 2.0×10^{17} ions/cm^2 for 100 nm, below 4.0×10^{17} ions/cm^2 for 50 nm and below 1.0×10^{18} ions/cm^2 for 25 nm. This can be certainly improved to reach diameter below 20 nm. But the nanographene amorphization is anyhow limiting down this diameter.

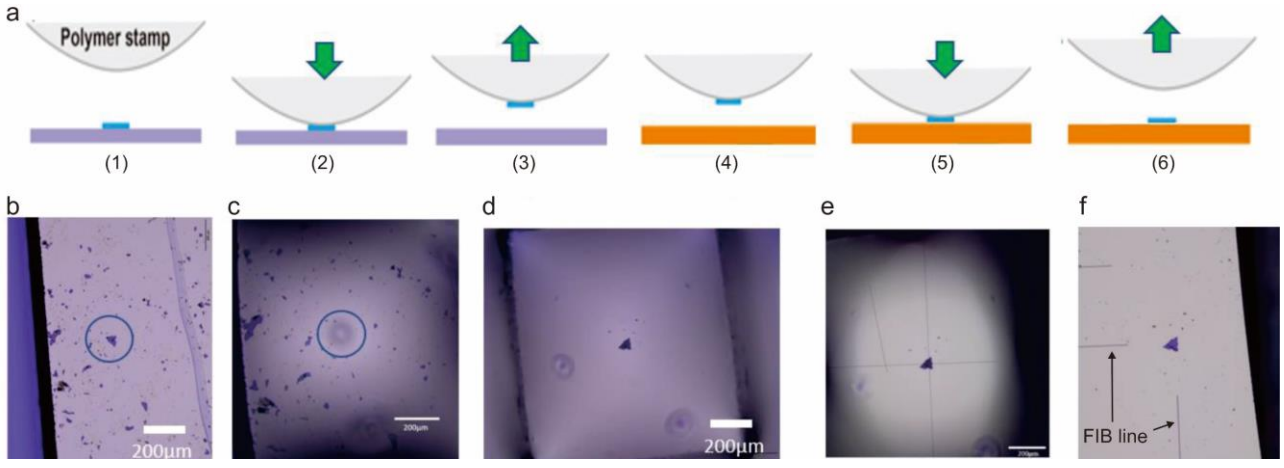

Figure 4. a) The graphene flake transfer. Selection of the HIM machined flake on the initial Au/Ti/sapphire substrate through the transparent stamp b). (2) Contacting the flake with the stamp. The optical image c) is focused on the surface while the flake is on the stamp surface. (3) Picking-up the selected flake. The optical image d) showing the stamp de-wetting the surface with the flake on its surface. (4) The change of surface for a new clean Au/Ti/ sapphire surface where FIB lines had been pre-fabricated to ease the location of the unique transferred flake for AFM imaging. (5) The transfer of the flake from the stamp to this new surface with the focused optical image on the stamp while an FIB line is also imaged top left. (6) The stamp retraction. The optical image f) showing the final selected position of the graphene flake at the end of FIB fabricated lines done before the stamping.

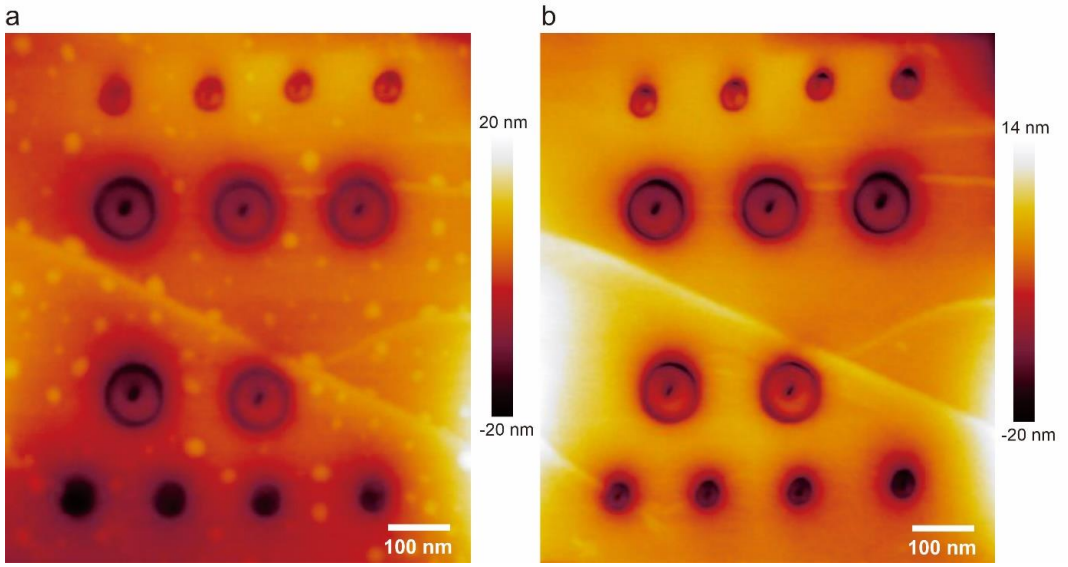

Figure 5. Tapping mode AFM image of the same HIM machined area of the transferred graphene flake a) before and b) after its surface cleaning in THF. Notice the white stripe along the surface indicative of the graphene surface stress caused by the HIM machining of the graphene nano-disks. The imaged nano-disks have 100 nm and 50 nm in diameter with their central hole for the rotation axle.

$N = 8$ was found to be optimum for cutting a $D = 100$ nm nano-disk, for controlling the heat generation and as a consequence the local graphene amorphization and vaporization (see Section 3). A constant He^+ ionic beam current between 0.2 pA and 0.5 pA was used for all the experiments. Following our first He^+ milling experiments on graphene, we take care of the stability of the He^+ emitting trimer on the tip of the microscope. This is an important point because a direct cutting is requiring large He^+ doses between 10^{17} and 10^{20} He^+ ions/cm^2 and because a complete process analysis required the sculpturing of hundreds of nano-disks with the same He^+ emitting tip. Doses larger than 10^{21} ions/cm^2 renders the emitting tip atomic structure unstable. Doses below 10^{17} ions/cm^2 are generally not operant for a direct cutting on a graphene 100 nm thick nanomaterial. The dwell time per pixel was adjusted to achieve the required dose. We have used a sapphire wafer to ease the heat dissipation generated by He^+ irradiations at high doses [9,10]

Going from 200 nm to 15 nm in diameter, a series of nano-disks is presented in figure 1 (first line) HIM imaged at low dose. When possible and depending on the nano-disk diameter, a central hole was also He^+ machined (figure. 1, second line). For this purpose and on this microscope, we have found that a gentle line by line irradiation with only 5-20 pixels per line and 5-20 lines is preferable than to stop the He^+ beam at the centre of the nano-disk for a long irradiation time as it was performed in [10]. The variation of the HIM measured graphene nano-disk diameters as a function of the programmed He^+ irradiation circle diameter D is presented in Fig. 2. This diameter is always smaller than D. For $D < 50$ nm, the difference is only 10 nm and for $D > 60$ nm, this difference becomes larger than 40 nm because of the $N = 0.08\ D$ irradiation followed strategy. To minimize this difference for large D, one strategy can also be to reduce N for large D. But it must be performed in a non-linear manner because of the heat generated by our He^+ machining (see section 3 for discussion).

As compared for example with an e-beam process using a resist, there are no proximity effects with our He^+ direct irradiation process. As a consequence, the figure 2 process characterization is presenting its D down limit almost reaching 10 nm for $N = 1$. For very optimized e-beam resist processes, the break occurs generally around 40 nm [14,15]. A free of resist machining is clearly here an advantage. It limits the nano-disk edge deformation and the amount of surface chemical impurities difficult to release for ultra-high vacuum applications like driving a single molecule-gear train [3,7]. Its drawback is the large irradiation dose required because a resist is playing the role of a sensitizer limiting the irradiation whatever the beam used (e-beam [8], ion-beam [12]). It has also the drawback of a very large increase of the surface local temperature which is transforming the machined nanomaterial up to its surface vaporization (See section 3).

As presented in figure 3, another way of characterizing our He^+ cutting process is to plot the variation of the HIM measured graphene nano-disk diameters as a function of the dose by using again low He^+ dose for HIM imaging. According to those curves, there is a down limit to our machining where no graphene cut occurs. To compensate and for $D < 50$ nm, the number of irradiated pixels per line can for example be increased with $N > 0.08\ D$ to cut more. But this is causing a large damage of the surrounding graphene surface. For $D > 50$ nm, an N increase is also possible but it has the consequence to heat up more the machined central disk and to favor the carbon vaporization as discussed below. The HIM imaging performed immediately after the machining and before exposing the sample to air is not sensible to the surface corrugation changes induced by the He^+ irradiations. The same curves plotted using AFM imaging are presented in figure 7. It shows that for machining doses larger than 5×10^{18}

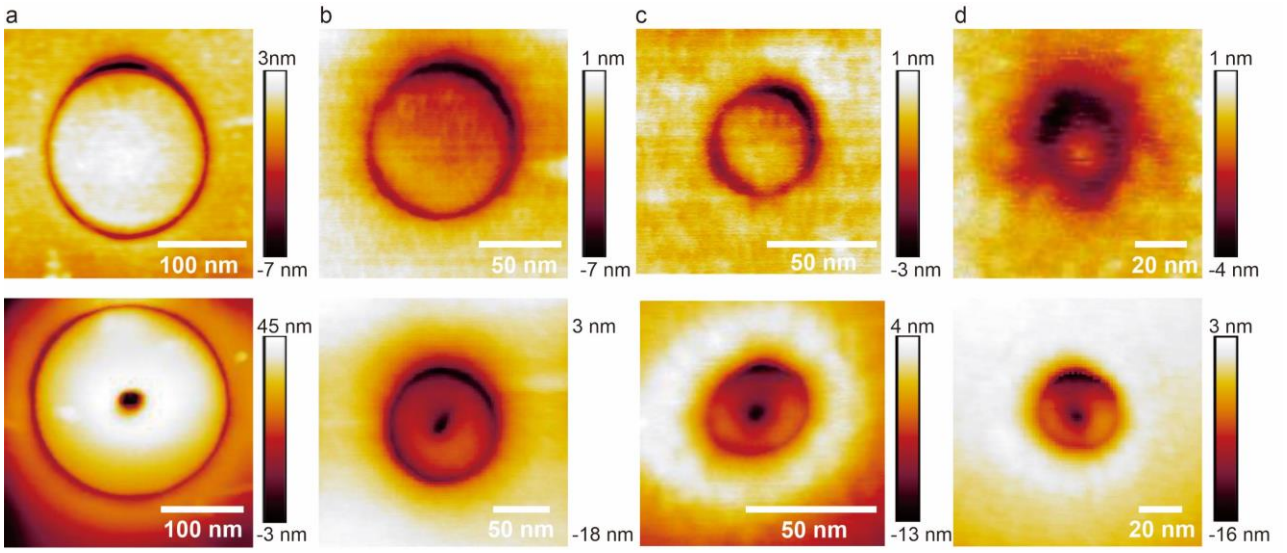

Figure 6. Tapping mode AFM images of a series of nano-disks of different diameters without and with their central hole. Diameters: from 200 nm to 15 nm with no central hole (top line) and from 500 nm to 30 nm with a central hole (bottom line) after the graphene flake transfer and the THF cleaning steps. Top d) is the residual of the amorphized graphene disk while down d) has a preserved diameter but is certainly amorphous too.

ions/cm^2, the nano-disks are becoming amorphous. The nano-disks can even be vaporized during the irradiation process. For HIM imaging, this can be observed only for $D < 50$ nm and at very large doses as indicated on the figure 3.

2.2. In air transfer printing and surface cleaning (3 different possibility)

For transferring an He^+ machined graphene flake from its original Au/Ti/Sapphire surface to a fresh one with the FIB fabricated marks for AFM imaging (see figure 4a), a modified version of the in-air dry transfer method was used [16]. First, the original Au/Ti/sapphire substrate with all its graphene flakes including the He^+ machined ones was mounted on the sample stage of our optical microscope-based transfer system [16]. A polymer stamp made of polypropylene carbonate (PPC)/polydimethylsiloxane (PDMS) deposited on a transparent glass plate (2.5 cm × 1.5 cm) was positioned on the manipulator mounted next to the sample stage (figure 4a(1)). The stamp and the He^+ graphene flake are put into contact by controlling the pressure using the manipulator (figure 4a(2)). After waiting 1 minute, the graphene flake was picked up from the original Au/Ti/sapphire substrate to the stamp by quickly retracting this stamp (figures 4a(2), 4a(3), and figures 4b-4d). Next, the fresh new Au/sapphire substrate was mounted on the sample stage in place of the original one while the stamp is still holding up the graphene flake (figure 4a(4)). Then, this stamp was contacted to the fresh Au/sapphire surface (figures 4a(5) and 4e). After waiting 5 minutes, the graphene flake can be detached from the stamp by slowly retracting the stamp. It remains onto the fresh Au/Ti/sapphire surface (figure 4a(6) and 4f). During the pick-up and drop steps, the stamp is optically transparent which ease the positioning of the stamp on the graphene flake to be transferred. The temperature of the sample stage was set to about 80°C. At this temperature, the viscosity of PPC decreases, facilitating the two transfers.

One consequence of using a PPC/PDMS stamp is that some polymer residues remain on the graphene flake surface (see for example figure 5a or figure 11b) after its transfer. In order to remove this surface contamination without moving the transferred graphene flake at its printed position, several cleaning processes were attempted like annealing the sample

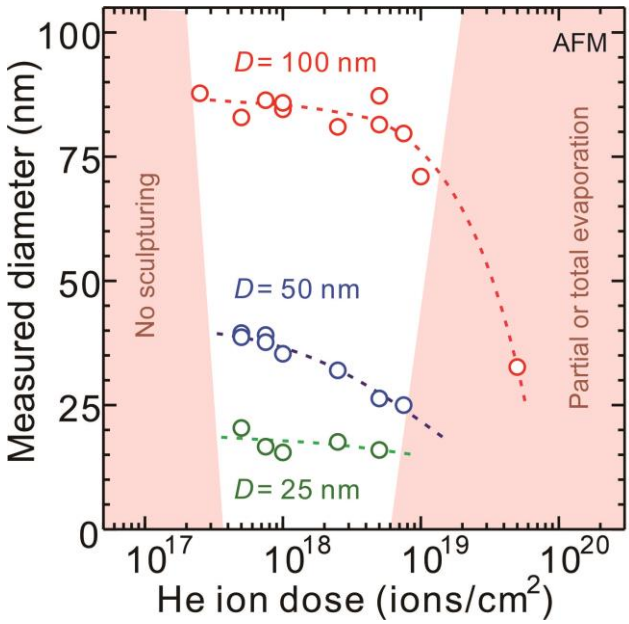

Figure 7. The variation of the AFM measured graphene nano-disk diameters as a function of the dose for three characteristics diameters: 100 nm, 50 nm, and 25 nm. Only the cases where the nano-disk are complete and vaporized partially are considered explaining for example the $D = 50$ nm slope.

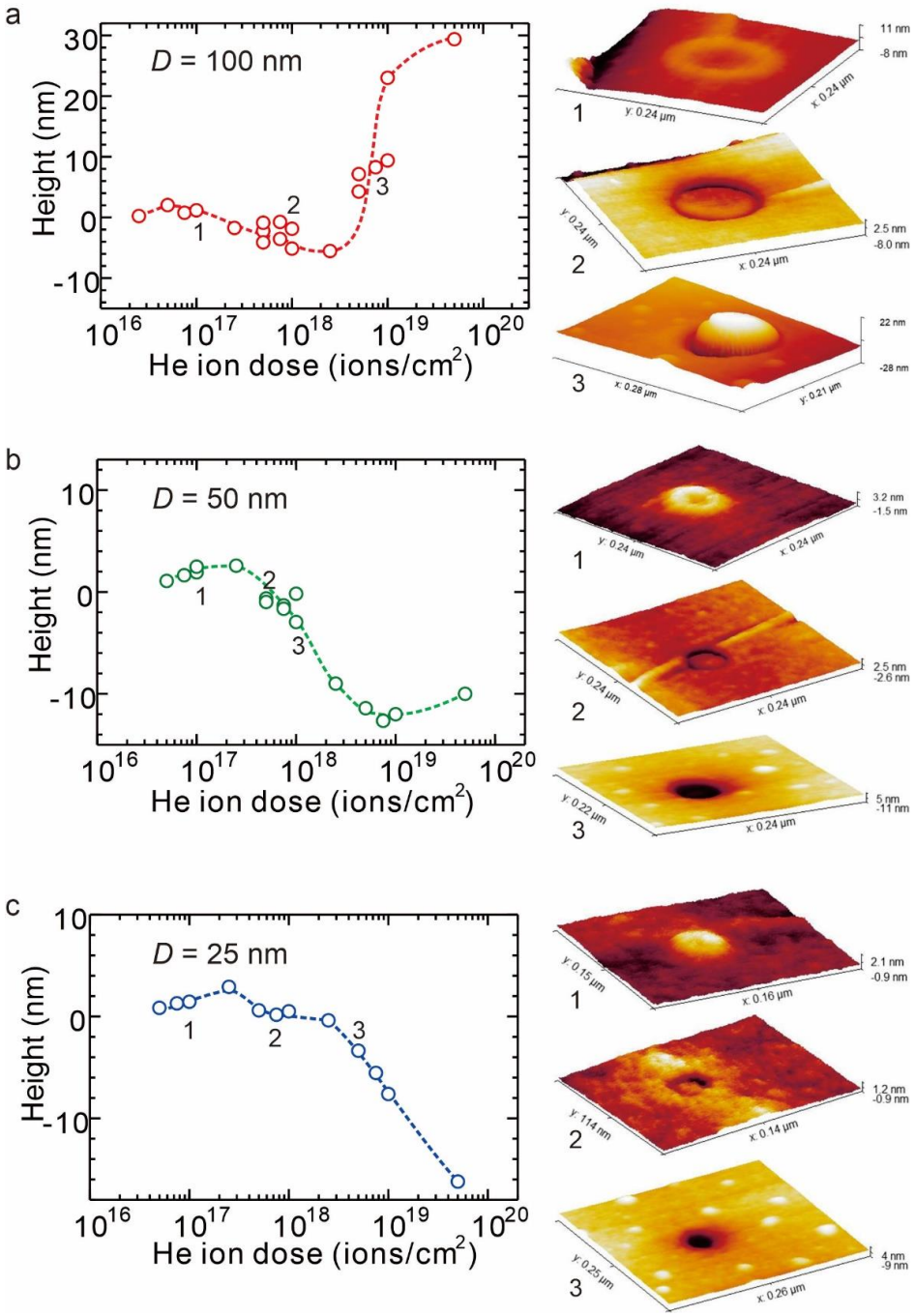

Figure 8. a)-c) The variation of the nano-disk height as a function of the HIM dose used for machining for three different cutting diameters. Down to 50 nm, nice graphene nano-disk can be observed as presented for D = 50 nm (AFM image 2). The 25 nm nano-disk are systematically found partially or totally vaporized by the HIM machining.

or using a moderate e-beam scanning dose to destroy those remaining. From the constrains of causing no damage to the nano-disk nanoscale structure, a simple dissolution process by an organic solvent was finally selected. First, the Au/sapphire substrate with its graphene flake was carefully rinsed two times by Tetrahydrofuran (THF). An ultrasonic bath cannot be used for keeping the flake on the surface. Then, it was immerged in THF more than 12 hours, rinsed again and dried in a vacuum desiccator. Figure 5 shows the AFM images before and after this cleaning procedure. All the PPC/PDMS polymer residues were removed from the graphene flake surface.

2.3. The nanodisk structure characterization

The above transfer and cleaning processes were developed to be able to use AFM images and to record detail line scans to complete the low dose HIM images as presented in figure 1.

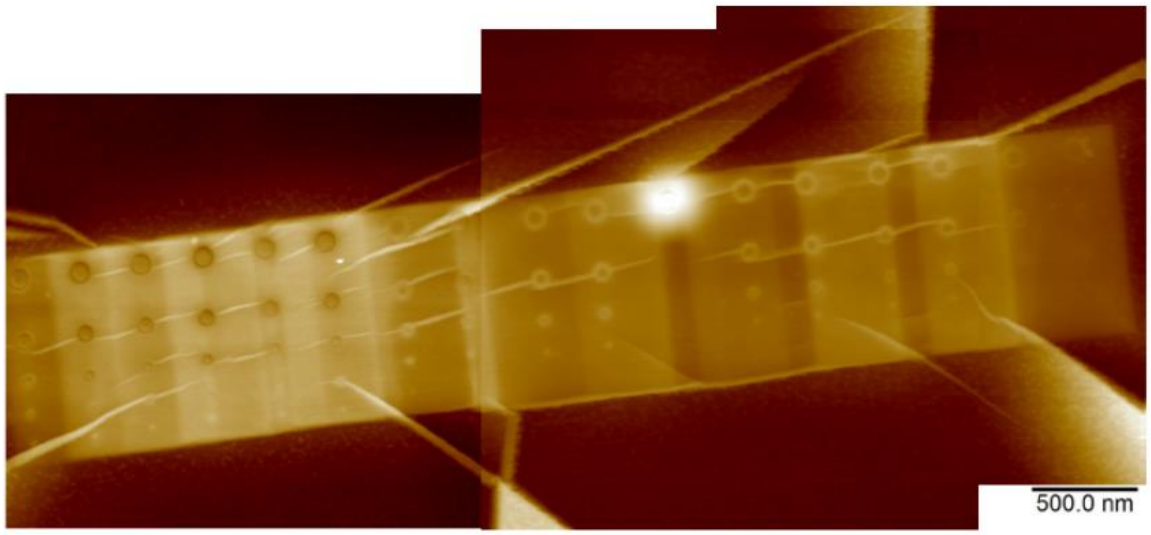

Figure 9. An assembly of 3 successive tapping mode AFM images (large scanning) recorded on a graphene nano-flake after its HIM machining. Large graphene surface deformation is observed ,all starting from the HIM machined area indicating that for this example, the nano-disks were machined too closed to each other. For each nano-disk row, top to down D = 100 nm to 25 nm. Different HIM He^+ dose have been tried in this example 1.0×10^{17} to 1.0×10^{19} ions/cm^2 from right to left respectively.

Using an optimized cutting dose and as presented in figure 6, He^+ machined graphene nano-disks down to D = 50 nm are very well defined. The limit of our process is 50 nm in diameter to obtain a flat graphene nano-disk surface. In figure 7, we have plotted the AFM equivalent of figure 3 now using AFM measured nano-disk diameters instead of HIM measurements. The comparison is indicating that while the cutting dose range to machine 100 nm flat surface nano-disks is quite large (from 2.0×10^{17} ions/cm^2 to 2.0×10^{19} ions/cm^2), it reduces very fast with D to reach almost only one dose value for D = 25 nm around 1.0×10^{18} ions/cm^2. As indicated above, one can also play with the number N of lateral irradiation pixels. But for D = 25 nm, reducing the dose to N = 1 single pixel will not lead to a clear top graphene surface cut.

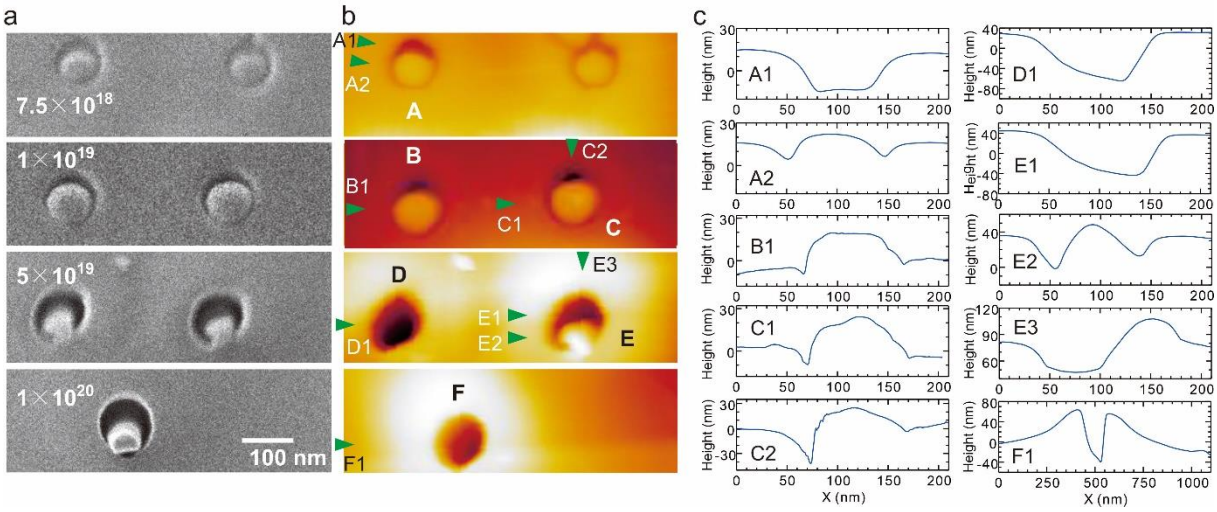

Figure 10. Examples of 100 nm in diameter graphene nano-disk vaporization (intermediate or total); a) Low dose HIM imaged during the HIM machining. b) The same nano-disks tapping mode AFM imaged after the graphene nano-flake transfer and cleaning on a fresh Au/Ti/Sapphire surface. c) Corresponding line profile of the AFM image arrowed in b). In a), the two 7.5×10^{18} ions/cm^2 dose nano-disks are perfectly machined as confirmed by their AFM image in b). According to a); the two 1.0×10^{19} and 5×10^{19} ions/cm^2 dose ones started to deform and vaporize. After their transfer, nano-disk A remains on the stamp. In a) and b), the carbon started to pile up from the resulting machined hole. After the transfer and cleaning, D and F are empty and the AFM scan gives a deepness of about 80 nm, a case not shown in figure 8a. The graphene layers partially amorphized at the bottom of the vaporized region are also removed with the residual in D, F of a) during the transfer and cleaning. It results in the formation of the large hole. Note that the dose of 1×10^{20} ions/cm^2 induces a wide protrusion of about 500 nm around the circle.

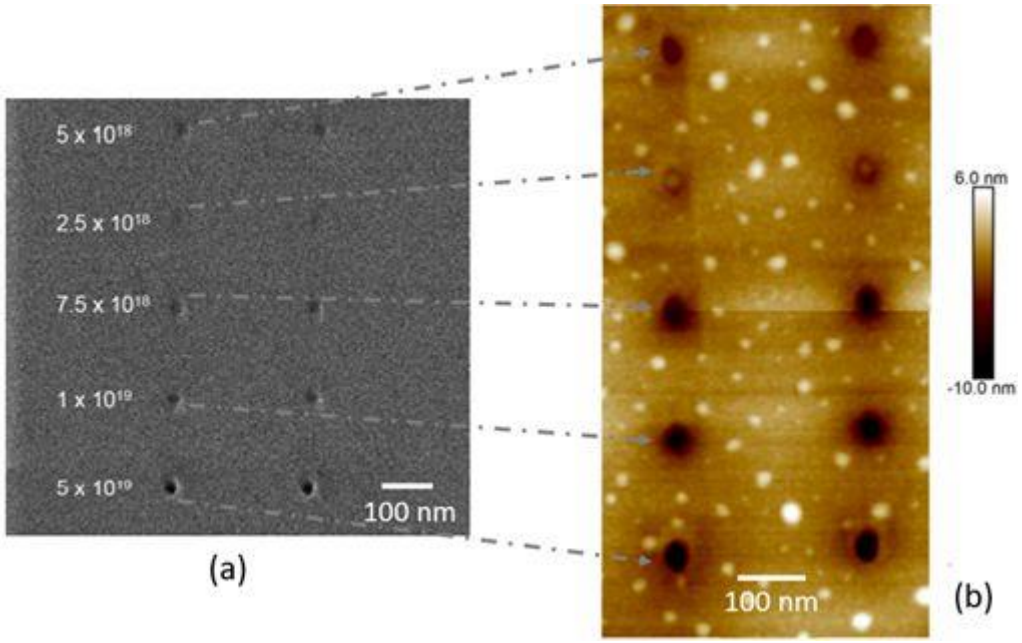

Figure 11. Example of the attempt to stabilize the HIM machining of 25 nm graphene nano-disks by varying the dose as shown in figure 1, 7 and 8. Two nano-disks were machined at each dose indicated in a) the low dose HIM image after the cutting and b) the corresponding tapping mode AFM image after the transferred but not THF cleaned. Only the 2.5×10^{18} ions/cm^2 dose results in nice $D = 20$ nm nano-disks with a flat surface according also to figure 8(b). Notice that the 5.0×10^{18} ions/cm^2 dose holes are not completely empty.

The variations of the nano-disk surface height relative to the graphene surface flake is plotted in figure 8 as a function of the dose. It confirms the irradiation conditions for preserving the graphene layers on top of the nano-disks. For $D = 100$ nm, we observed a top surface height increase at large doses, opposite to what we observed at small D where here empty of carbon hole are found at the nano-disk location. As discuss below, this phenomenon is caused by a competition between the progressive amorphization of the top graphene layer of the nano-disk (confirmed below by TEM electron diffraction pattern measurements) and the presence of a possible carbon liquid phase underneath the top layer nano-disk surface. Frozen after stopping the irradiation because of the fast sapphire surface cooling effect, this liquid phase is confirmed by the observation that carbon droplets have been left on the original Au/Ti/sapphire surface during the transfer process described in section 3.

We have also performed large scan tapping mode AFM images and observed large graphene surface mechanical deformations propagating far away from the nano-disks machined locations (figure 9). When the distance between two machined nano-disks is small, typically below 200 nm, a lot of surface stress are created around the machined area (figure 9), pointing out the requirement to separate each machining operation by at least a 500 nm distance.

3. Discussion

At irradiation doses larger than 1×10^{17} ions/cm^2, the He^+ cut process is exothermic. This machining is locally generating heat like in any macroscopic machining process and also like machining surfaces using Ga^+ field ion beam [17,18,19]. Even performed on a sapphire wafer, used here on purpose to evacuate the surface heat as fast as possible, it induces a large temperature increase [9]. There are many different consequences of this large temperature increase on the graphene surface (and underneath the top surface layers) in reference to the very high thermodynamic triple point (P,T) of carbon macroscopic materials [20].

All the machining experiments described above were performed at 10^{-6} Torr. At this low pressure and according to the position of the carbon materials (P,T) on its thermodynamic phase diagram [20], the only phase transition at this low pressure is a solid to gas phase transition. The consequence of this low 10^{-6} Torr pressure is the vaporization of carbon atoms from the surface. The macroscopic carbon (P,T) position is well known but not the one for nanoscale carbon [21]. At this 10^{-6} Torr pressure, it is difficult to anticipate how this triple point will go down when for example reducing the carbon nanomaterial size down to a 100 nm × 40 nm carbon cylinder (figure 10). This explains how at very high He^+ cutting dose, only empty holes can be imaged even for a 100 nm expected nano-graphene nano-disk (see the interesting figure 10 case where a 100 nm nanodisk start to vaporize during its HIM machining and remains on the transfer stamp at the transfer step). It is like having fabricated a nano-crucible full of carbon, cooled down by its back-sapphire support and vaporizing out carbon atoms at 10^{-6} Torr due the very local increase of its temperature. Except for extremely high doses, the crucible diameter was nearly constant because the heat generated by the dose propagated quickly in the lateral direction due to the high thermal conductivity of graphene.

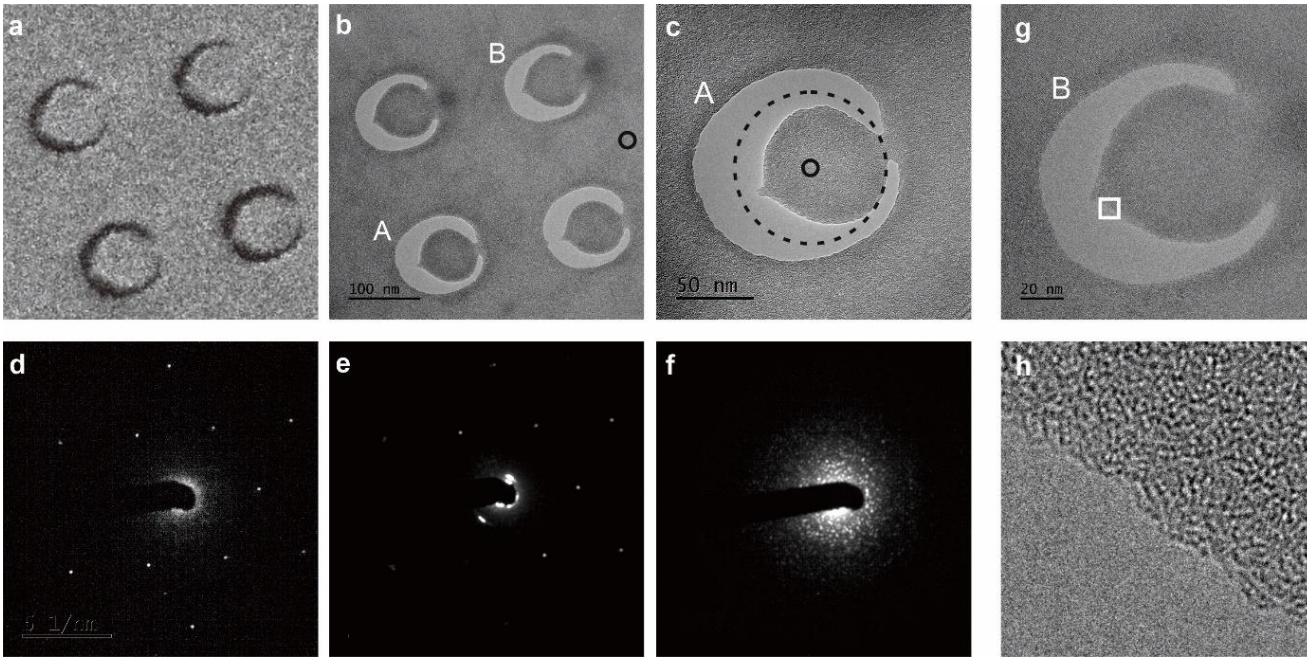

Figure 12. a) HIM image of graphene nano-disks machined with left: 5×10^{18} ions/cm^2 and right: 6×10^{18} ions/cm^2, b) a TEM image (JEOL, JEM-ARM200F, 80 kV) of exactly the same area, c) a magnified TEM image of the down left designed 100 nm graphene nano-disk A in b). The black doted circle is indicating the D = 100 nm programmed HIM cut. Bottom line images from d) to f): TEM diffraction pattern recorded with a 10 nm e-beam scanning diameter. d) The reference diffraction pattern recorded on the graphene away from the HIM low dose scanning. e) The pattern recorded on the HIM scanned area indicated on b) by a black circle and after the HIM scanning and machining. f) The pattern recorded exactly at the center of the HIM machined nano-disk TEM imaged in c) black circle (d = 10 nm). g) The magnified TEM image of the top right designed 100 nm graphene nano-disk B in b) and h) a high-resolution TEM image showing the regular edge on the resulting nano-disk (recorded at white square in g)).

In some cases, it is also intriguing to be able to image (HIM, AFM) carbon nanomaterials residues deep down a resulting graphene hole as if an intermediate liquid phase had existed before freezing and bringing the sample to air [22]. Pressure under the first graphene layers is high because only a small expansion of the other layers below the surface can occur. In that case, a liquid phase can be formed underneath the surface during the irradiation [22]. The large volume expansion and deformation of the graphene in the nano-disk (figures 8a and 10) indicate that the graphene during the irradiation is in a liquid phase. It is limited in depth because of the high thermal conductivity of graphene explaining why the maximum AFM measured hole depth was never larger than 80 nm with an average of 20 nm. Furthermore, and as soon as the top graphene layer is vaporizing, less and less carbon atoms are available underneath the top surface to form the liquid phase. This explains how only small frozen carbon nano-droplets remains at the bottom part of the holes for small nano-disks (figure 11). For large nano-disk diameters and during the irradiation, this carbon liquid phase is pushing up the nano-disk graphene top surface before freezing while in air (figure 10).

For moderate cutting doses, nano-disks between 100 nm and 50 nm in diameter are machined with a rather top flat surface (see figures 6 and 8) and the same for a 25 nm diameter only in a very limited number of cases. In those cases, a partial integrity of the graphene is maintained. Our interpretation here is that for a moderate dose, only a partial amorphization of the graphene nano-disk occurs.

To certify this point and for the same He^+ dose range used above, we have performed an He^+ nano-disk machining on a double layer graphene CVD deposited on a TEM grid. This allows us to obtain e-beam diffraction patterns [23] with here an electron beam spot size of about 10 nm on our new JEOL-ARM 200F electron microscope. As presented in figure 12 and depending on the e-beam spot position, one can follow the progressive amorphization of the graphene double layer as a function of the electrons spot distance from the machined graphene nano-disk. The advantage of this technique is that the direct space TEM image of the same nano-disk can also be obtained to correlate the different diffraction patterns with the e-beam spot position on, near and far away from this graphene nano-disk. The experimental difficulty here is that for a small 10 nm spot size, the electrons accumulation time to get a complete diffraction pattern is more than 120 s. During this time laps, inelastic electronic effects are very active even at extreme low current intensity ($\gtrsim$ 5 pA/cm^2). This has the drawback to step by step decompose the graphene nano-disk from the edge as we have observed in real time during the TEM images recording. As a consequence, those very local diffraction experiments are only one-shot experiments. In any case, they confirm the amorphization for doses larger than 5.0×10^{18} ions/cm^2 of the nano-disk structures and also around the machined area.

Those TEM images open also the opportunity to get high resolution images at the border of a given graphene nano-disk (figure 12h). Those images confirm how the nano-disk graphene edge corrugation is less than a nanometer certainly because of the vaporization process. This is a positive point in regard to solid state nano-gears application to drive the rotation of a single molecule-gear [3].

4. Conclusion

Focused He^+ ions beam direct machining was used on the surface of a graphene multilayer deposited on an Au/Ti/sapphire support to explore the limits of graphene solid-state nano-disk fabrication for approaching the molecular scale. Without any resist, for the purpose to reach a better precision i.e. at irradiation doses larger than 5.0×10^{17} ions/cm^2 and with an He^+ beam size well below 1 nm, graphene disks down to 20 nm in diameter have been obtained. The local heat generated by this irradiation is inducing a partial graphene amorphization and deformation at doses closed to this threshold. It leads to a complete graphene nano-disk vaporization at larger doses for the vacuum pressure required for the He^+ beam generator functioning. For nano-disk down to 50 nm in diameter, a central hole can also be machined for preparing the positioning on a rotation axle. A dry transfer printing like technique followed by a graphene surface cleaning was used to transfer a well identified single graphene flake where the nano-disks have been machined from its initial machining surface to a fresh and clean surface where FIB marks have been fabricated in anticipation to ease the AFM tip positioning. Tapping mode AFM have been recorded to follow how the vaporization occurs as a function of the He^+ dose used. Starting already during the 50 nm graphene nano-disks fabrication, this vaporization limits the nano-disk diameter down to 20 nm on graphene. Since graphene was selected to reach nano-disks with an atomic scale thickness to be compatible with the mechanics of single molecule machinery, this limit points out the need to explore other 2D materials to also be compatible in thickness with single molecule-gears and motors. In particular, 2D nanomaterials with heavy metal atoms like MoS_2 can be a better choice to limit the vaporization phenomenon observed on graphene. Considering now how to use the obtained nano-hole in graphene, our process can be also used to fabricate metal-surface [24] and grating [25]. In this direction, new 2D materials like black phosphorus [26,27] are also of interest for HIM milling.

Data availability

The data that support the findings of this study are available from the corresponding authors upon reasonable request.

Declaration of Competing Interest

The authors declare that they have no known competing financial interests or personal relationships that could have appeared to influence the work reported in this paper.

Acknowledgements

This work was supported in part by the World Premier International Center (WPI) Initiative on Nanoarchitectonics (MANA), MEXT, Japan and in part by the European FET-Open project MEMO (Grant N°766864). We thank Dr. Nemoto Y for giving us access to the JEOL transmission electron microscope to perform the electronic diffraction experiments and Dr. IIjima T for the operation of a helium ion microscope supported by nano-processing facility in AIST-NPF. This work was supported by NIMS Materials Fabrication and Analysis Platform, Electron Microscopy Unit. This is partially supported by Advanced Research Infrastructure for Materials and Nanotechnology in Japan (ARIM) of the MEXT (Grant Number: JPMXP1222BA0047).

Reference

[1] Joachim C 2020 in" Building and Probing Small for Mechanics", Springer Series: *Advances in Atom and Single Molecule Machines*, Vol. XIII, p.1

[2] Srivastava S, Kino H, Joachim C, 2017 *Chem. Phys. Lett.*, **667** 301-306.

[3] Soe W H, Srivastava S, Joachim C, 2019 *J. Phys. Chem. Lett.*, **10** 6462-6467.

[4] Yeung K H A, Kühne T, Eisenhut F, Kleinwächter M, Gisbert Y, Robles R, Lorente N, Cuniberti G, Joachim C, Rapenne G, Kammerer C, Moresco F, 2020 *J. Phys. Chem. Lett.* **11** 6892-6899.

[5] Perera U G E, Ample F, Kersell H, Zhang Y, Vives G, Echeverria J, Grisolia M, Rapenne G, Joachim C, Hla S - W 2013 *Nature Nano*. **8** 46-51.

[6] Ohmann R, Meyer J, Nickel A, Echevaria J, Joachim C, Moresco F, Cuniberti G, 2015 *ACS Nano* **9** 8394-8400.

[7] Lin H H, Croy A, Gutierrez R, Joachim C, Cuniberti G, 2022 *Nanotechnology* **33** 175701.

[8] Yang J, Deng J, Troadec C, Ondarcuhu T, Joachim C, 2014 *Nanotechnology* **25** 465305.

[9] Sakurai M, Nagano S, Joachim C, 2020 *Nanotechnology* **31** 345708.

[10] Sakurai M, Nagano S, Joachim C, 2023 *Vacuum* **207** 111605.

[11] Yun Y J, Ah C S, Kim S, Yun W S, Park B C, Ha D H, 2007 *Nanotechnology*, *18*, 505304.

[12] Mailly D, Faini G, 2020 in" Building and Probing Small for Mechanics" Springer Series: *Advances in Atom and Single Molecule Machines*: Vol. XIII, p.41.

[13] Verveniotis E, Okawa Y, Nakaharai S, Ogawa S, Nakayama T, Aono M, Joachim C, 2019 *Jpn. J. Appl. Phys.* **58** 055007.

[14] Cholet S, Joachim C, Martinez J P, Rousset B, 1999 *Eur. Phys. J. Appl. Phys* **8** 139-145.

[15] Saifullah M S M, Ondarcuhu T, Koltsov D F, Joachim C, Welland M, 2002 *Nanotechnology* **13** 659.

[16] Iwasaki T**,** Endo K, Watanabe E, Tsuya D, Morita Y, Nakaharai S, Noguchi Y, Wakayama Y, Watanabe K,

Taniguchi T, Moriyama S, 2020 *ACS Appl. Mater. Interfaces* **12** 8533-8538.
[17] Ishitani T, Yaguchi T 1996 *Microscopy Research and Technique* **35** 320-333.
[18] Park Y, Park S, Lee U, Choi S H 2010 *Recent Patents on Space Technology* **2** 51.
[19] Wolff A, Klingner N, Thompson W, Zhou Y, Lin J, Peng Y Y, Ramshaw J A M, Xiao Y 2018 *Journal of Microscopy* **272** 47-59.
[20] Haaland D M 1976 *Carbon* **14** 357-361.
[21] Los J H, Zakharchenko K V, Katsnelsoln M I, Fasolino A 2015 *Phys. Rev. B* **91** 045415.
[22] Xia W, Vargas-Lara F, Keten S, Douglas J F 2018 *ACS Nano***12** 5427-5435.
[23] Meyer J C, Geim A K, Katsnelson M I, Novoselov K S, Booth T J, Roth S 2007 *Nature* **446** 60-63.
[24] Lee S and Kim S, 2023 *Appl. Sci*.**13** 9708.
[25] Valagiannopoulos C A, Tretyakov S A, 2014 *EEE Trans. Ant. Prop.* **62** 5089-5098.
[26] Valagiannopoulos C A, Mattheakis M, Shirodkar S N, Kaxiras E 2017 *J. Phys. Commun.* **1** 045003.
[27] Wu Z, Lyu Y, Zhang Y, Ding R, Zheng B, Yang Z, Lau S P, Chen X H, Hao J 2021 *Nat. Mater*. **20** 1203-1209.